Computers and Electronics in Agriculture 235 (2025) 110321

Contents lists available at ScienceDirect

Computers and Electronics in Agriculture

journal homepage: www.elsevier.com/locate/compag

Original papers

Neural network estimation of thermal conductivity across full saturation for various soil types

Yongwei Fu [a,b,c,*], Robert Horton [d], Joshua Heitman [c,*]

[a] College of Land Science and Technology, China Agricultural University, Beijing 100193, China
[b] Key Laboratory of Arable Land Conservation in North China, Ministry of Agriculture and Rural Affairs, Beijing, China
[c] Department of Crop & Soil Sciences, North Carolina State University, Raleigh 27695, United States
[d] Department of Agronomy, Iowa State University, Ames 50011, United States

ARTICLE INFO

Keywords:
Thermal conductivity
Water content
Neural network
Pedotransfer function
Hyperparameter tuning

ABSTRACT

Soil thermal conductivity (λ) relates directly to heat conduction in soil. Numerous models have been developed to estimate soil thermal conductivity, but their applicability is often limited to specific types of soils. Recognizing the similarity between the soil water retention curve and the λ versus water content (θ) curve, Lu and Dong presented a λ(θ) model, which can provide accurate λ estimates for various soils but does not converge to the thermal conductivity value of a saturated soil (λ_{sat}) at saturation. In this study, we develop a modified form of the Lu and Dong (MLD) model. Additionally, we present a neural network (NN) approach to estimate parameters of the MLD model using soil porosity, sand, silt, and clay contents, as well as the thermal conductivity of soil solids (λ_s) as input features. The neural network is trained to optimize the hyperparameters, which are used to establish the NN-MLD model after the hyperparameter tuning process is completed. The NN-MLD model is then tested with an independent testing dataset and compared with five pre-existing models taken from the literature. Results show that the NN-MLD model outperforms the other models across four error metrics with a normalized root mean square error (NRMSE) of 0.049, a mean absolute error (MAE) of 0.098 W m^{-1} K^{-1}, an Akaike's information criterion (AIC) of −1699 and a coefficient of determination (R^2) of 0.94. In addition, error analysis across varying degrees of saturation (*S*) reveals that the NN-MLD model consistently outperforms the other models across the entire range of saturation levels and its superiority is most pronounced at medium levels of saturation, where the other models yield NRMSEs and MAEs values three times larger than those of the NN-MLD model. The NN-MLD model is available in Python code in the Supplementary Material.

1. Introduction

Soil thermal conductivity (λ) relates to a soil's ability to transmit heat by conduction. Soil thermal conductivity is widely used for interpretation and prediction of heat transfer processes and soil temperature in many fields including soil science, agronomy, civil engineering, and agricultural meteorology (Kojima et al., 2021; Al-Shammary et al., 2022). The magnitude of λ depends on inherent soil properties such as particle size distribution and mineralogy (Campbell et al., 1994) and dynamic properties such as soil water content (θ), temperature, porosity (ϕ), and soil structure (Abu-Hamdeh and Reeder, 2000).

Among these factors, water content (θ) has been shown to play a particularly important role in determining soil λ. Therefore, many efforts have been made to develop λ(θ) models. Based on empirical fits to natural soil measured values, many empirical models have been presented to describe λ(θ) relationships based on easily measurable soil properties (Johansen, 1975; Lu et al., 2007). These empirical models used logarithmic, exponential, or power functions with empirical parameters to fit measured values. Each model was generally only valid for limited types of soils or limited ranges of saturation, and their parameters lacked physical meaning. In addition, theoretical models were developed by conceptualizing the three-phase soil (i.e., solid, water and air) as a combination of series and parallel systems in the cubic cell or representative elementary volume, and mathematical models which were adopted from models of other physical properties (e.g., electrical conductivity and dielectric permittivity) (Campbell et al. 1994; Haigh, 2015). However, none of these models included the effects of soil microstructure (i.e., particle geometry, particle/pore size distribution,

* Corresponding authors at: College of Land Science and Technology, China Agricultural University, Beijing 100193, China (Y. Fu).
E-mail addresses: yfu@cau.edu.cn (Y. Fu), jlheitma@ncsu.edu (J. Heitman).

https://doi.org/10.1016/j.compag.2025.110321
Received 29 October 2024; Received in revised form 7 February 2025; Accepted 18 March 2025
Available online 28 March 2025

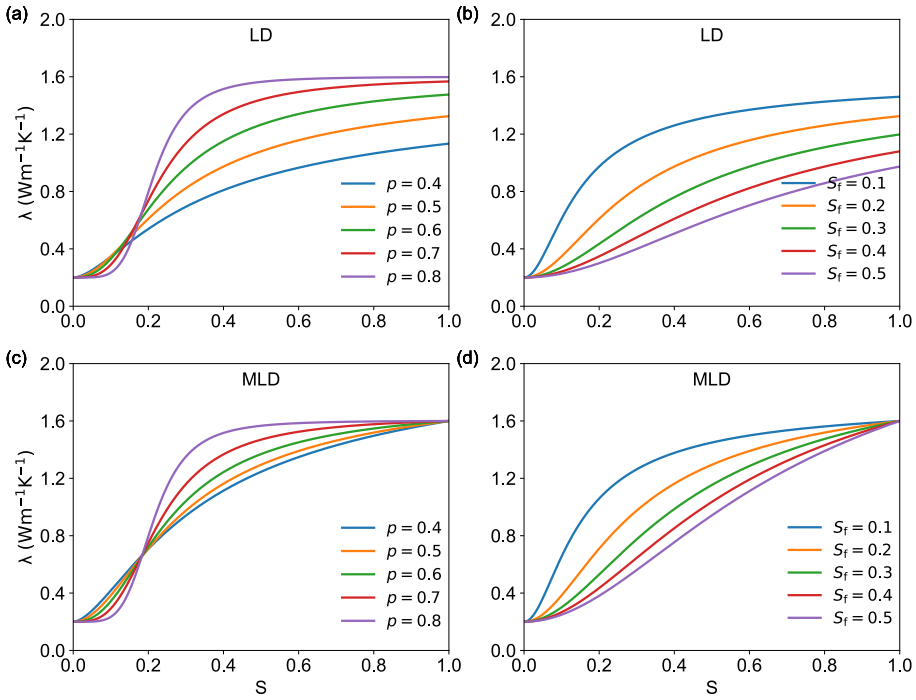

Fig. 1. Thermal conductivity (λ) versus degree of saturation (S) curves for various values of the shape parameter m and funicular water content S_f fitted with LD and MLD models, respectively. The default λ_{dry}, λ_{sat}, S_f and p values are set at 0.2 W m^{-1} K^{-1}, 1.6 W m^{-1} K^{-1}, 0.2 and 0.5, respectively.

pore-water arrangement and air–water interfaces) on the λ(θ) relationship.

There are some attempts to develop λ(θ) models based on the linkage between soil water retention mechanisms and corresponding thermal conductivity behaviors (Lu and Dong, 2015). A soil water retention curve (SWRC) is defined as the relationship between the soil water matric potential and the soil water content, which has four regimes (i.e., hydration, pendular (discontinuous water), funicular (continuous water) and capillary) based on capillarity and adsorption mechanisms (Tuller et al., 1999). These four water retention regimes can also be used to reconcile variations of λ with respect to θ for many types of soil. Considering these relationships, Lu and Dong (2015) proposed a sigmoidal λ(θ) function with two fitting parameters (i.e., funicular water content and a pore fluid network connectivity parameter). He et al. (2017) showed that among 38 models, the Lu and Dong (2015) model is among the best for fitting λ(θ), especially for fine-textured soils. However, the Lu and Dong (2015) model does not provide a proper thermal conductivity value for the saturated soil condition, meaning $\lambda \neq \lambda_{sat}$ (Sadeghi et al., 2018). Thus, improvements on the model are needed.

There is a growing demand for high-resolution soil parameter estimation, which is essential to improve land surface representations and predictions. The development of pedotransfer functions (PFTs) allows for the estimation of model parameters using easily measurable, fast and cost-effective soil properties. By integrating PTFs with grid-based soil data into land-surface models, it becomes possible to describe soil processes and parameterize them at larger scales (Van Looy et al., 2017). Many PTFs have been developed to estimate soil physical properties such as hydraulic properties (Zhang and Schaap, 2017; Navidi et al., 2022), electrical properties (Xiao et al., 2023; Sodini et al., 2024) and thermal properties (Li et al., 2022), or chemical properties like cation exchange capacity (Saadat et al., 2018; Jalali et al., 2019). These PTFs are designed either to estimate the parameters of the existing models—known as parametric PTFs—or directly relate predictors with target values (e.g., θ or λ) using machine learning algorithms, without assuming any pre-existing λ(θ) or hydraulic functions. Parametric PTFs provide limited accuracy because the uncertainty in a single PTF to estimate each parameter inevitably introduces errors into the final estimated values (Rudiyanto et al., 2021). In contrast, while machine learning algorithms may provide improved estimations by directly relating predictors to target values, their black-box nature often limits interpretability, hindering broader application (Shen et al., 2023).

The objectives of this study are as follows: first, we aim to develop a modified form of the Lu and Dong (2015) model to address its previously identified shortcomings; second, we use an artificial neural network to estimate the parameters of the newly developed modified λ(θ) model with soil basic properties; finally, we evaluate the performance of the modified model, with its parameters estimated via the established PTFs, by comparing its ability to estimate λ-values against values estimated by five pre-existing λ(θ) models.

2. Model development

2.1. *Lu and Dong (2015) model*

SWRCs and λ versus degree of saturation (S) curves have sigmoidal shapes. Based on observations and characteristics of the sigmoid function, Lu and Dong (2015) proposed a closed-form equation analogous to the van Genuchten (1980) model to describe the λ(S) curve,

$$\frac{\lambda - \lambda_{dry}}{\lambda_{sat} - \lambda_{dry}} = 1 - \left[1 + \left(\frac{S}{S_f}\right)^{1/(1-p)}\right]^{-p} \quad (1)$$

where λ_{sat} and λ_{dry} are thermal conductivity values of saturated soil and dry soil, respectively. S_f represents the degree of saturation at the onset of the funicular regime, where the menisci are fully interconnected. Beyond S_f, any further increases in S will continuously increase λ, though the contributions from pore water become less significant. Parameter p ($0 < p < 1$) is defined as the pore fluid network connectivity parameter for the λ(S) curve. Compared to other empirical models, the Lu and Dong (2015) model is the only one that captures well the sigmoidal shape of the λ(S) curve, especially for fine-textured soils (Sadeghi et al., 2018).

Although the LD model (Eq. [1]) can accurately describe λ(S) curves for many types of soils and outperforms other empirical models, it still

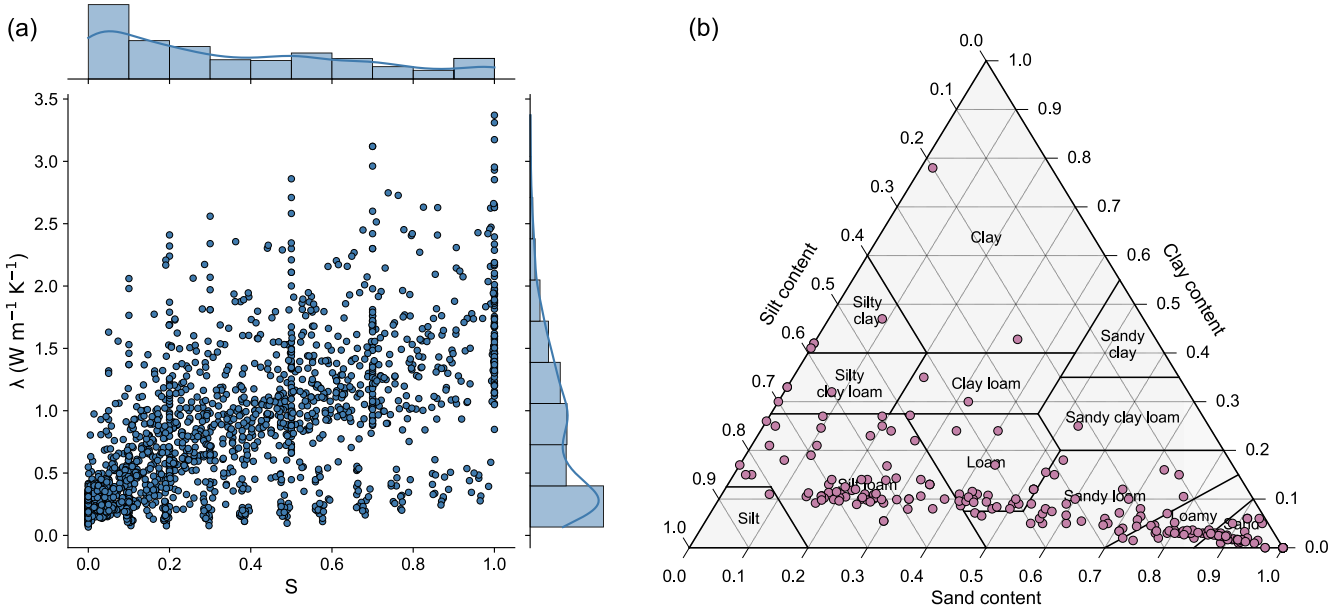

Fig. 2. (a) λ(*S*) data of the soils in the dataset used in this study and (b) Dataset soil samples (circles) distributed across U.S. Department of Agriculture (USDA) textural classes.

has some limitations. First, the LD model cannot satisfy the saturated soil condition ($S = 1$) where λ should equal λ_{sat}. In other words, λ converges to λ_{sat} only when *S* reaches infinity, which is unrealistic. This limitation becomes more pronounced with decreasing *p* or increasing S_f (Fig. 1a and 1b), particularly for fine-textured soils.

Parameters S_f and *p* have been reported to be correlated to the residual degree of saturation and the shape parameter of the van Genuchten (1980) model, respectively (Lu and Dong, 2015; Fu et al., 2021). However, SWRCs are not readily available for most soils, and this limits the practical application of the Lu and Dong (2015) model to estimate the λ(*S*) curve. Instead, if PTFs can be established to estimate the parameters in the Lu and Dong model, the usability and accuracy of the model can be significantly enhanced, allowing for more reliable estimations across various soil types and conditions.

2.2. The modified Lu and Dong model

To address the limitation when *S* approaches 1, we introduced a correction term into Eq. [1], leading to the following modified Lu and Dong (MLD) model:

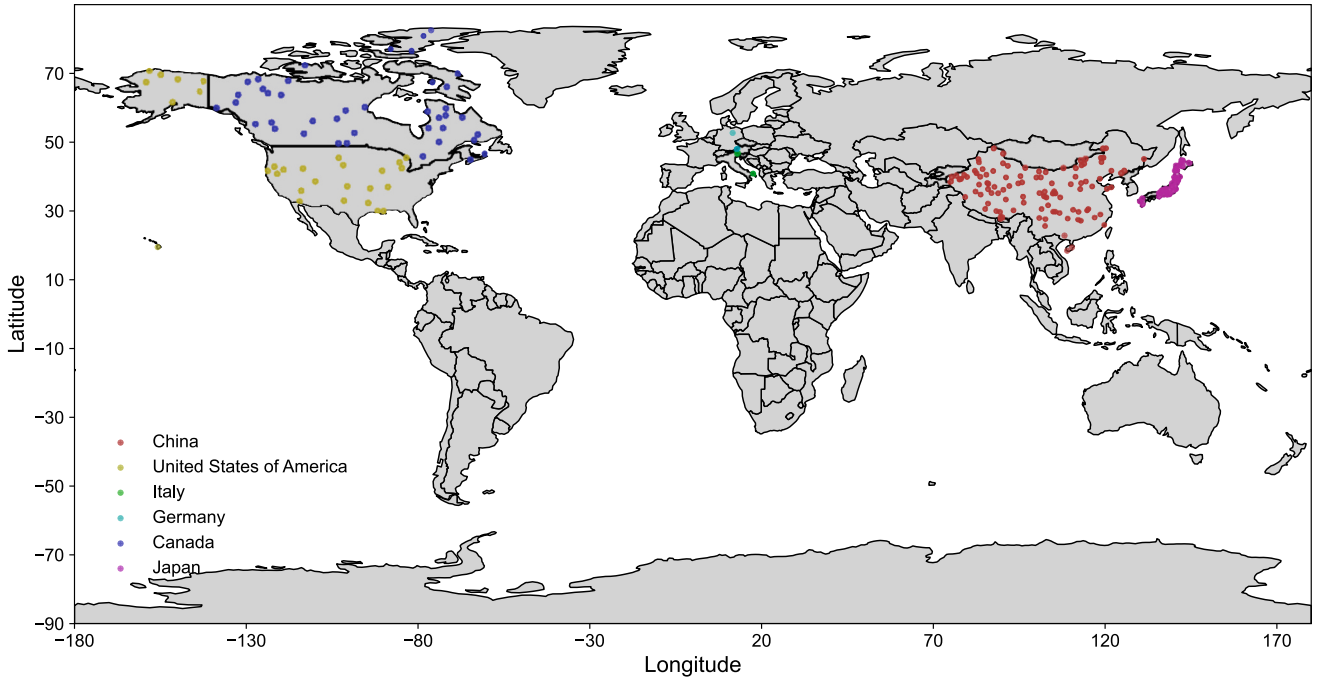

Fig. 3. Sampling locations of soil samples included in the dataset used in this study. Note that data points indicate the source countries rather than exact locations and are scattered for improved visualization.

Table 1
Ranges of degree of saturation (S) and thermal conductivity (λ), measurement methods, number of $\lambda(S)$ pairs, locations, and data sources complied in this study.

ID	S range	λ range	Method	Number of $\lambda(S)$ pairs	Origin	Sources
		W m^{-1} K^{-1}				
1	0–1.00	0.18–2.19	Transient heat transfer	140	China, US	Lu et al. (2007)
2	0–1.00	0.19–2.63	Transient heat transfer	116	China, US	Fu et al. (2021)
3	0–1.00	0.27–2.04	Transient heat transfer	30	Japan	Tokoro et al. (2016)
4	0–1.00	0.18–1.49	Transient heat transfer	22	Germany	Hailemariam et al. (2017)
5	0–0.62	0.15–1.36	Transient heat transfer	76	US	McInnes (1981)
6	0.02–0.71	0.12–1.30	Transient heat transfer	88	US	Campbell et al. (1994)
7	0.01–0.85	0.28–1.74	Transient heat transfer	8	US	Hopmans and Dane (1986)
8	0–1.00	0.25–3.37	Transient heat transfer	25	Japan	Kasubuchi et al. (2007)
9	0–1.00	0.11–2.63	Transient heat transfer	28	Japan	Mochizuki et al. (2003)
10	0–1.00	0.15–1.40	Transient heat transfer	40	Japan	Tarnawski et al. (2013)
11	0–1.00	0.13–3.17	Transient heat transfer	240	Canada	Tarnawski et al. (2015)
12	0–1.00	0.23–3.36	Transient heat transfer	12	Canada	Nikolaev et al. (2013)
13	0–1.00	0.19–1.20	Transient heat transfer	12	Italy	McCombie et al. (2016)
14	0–0.99	0.08–0.59	Transient heat transfer	204	Japan	Tarnawski et al. (2019)
15	0–1.00	0.07–2.95	Transient heat transfer	638	China	Zhao et al. (2018)
16	0–1.00	0.14–2.75	Steady state	165	US	Kersten (1949)

$$\frac{\lambda-\lambda_{dry}}{\lambda_{sat}-\lambda_{dry}}=\frac{1-\left[1+\left(\frac{S}{S_f}\right)^{1/(1-p)}\right]^{-p}}{1-\left[1+\left(\frac{1}{S_f}\right)^{1/(1-p)}\right]^{-p}} \quad (2)$$

with Eq. [2] fulfilling the dry and saturated soil conditions:

$$S\to 0;\lambda=\lambda_{dry} \quad (3a)$$

$$S\to 1;\lambda=\lambda_{sat} \quad (3b)$$

As illustrated in Fig. 1b and 1d, the MLD model mirrors the sigmoid shape of the $\lambda(S)$ curves, which effectively capture both the 'flat tail' at the hydration regime and the drastic onset of the pendular regime. Moreover, the MLD model reliably returns $\lambda = \lambda_{sat}$ when $S = 1$, regardless of the values of p and S_f, ensuring consistent behavior across different combinations of parameters.

In the following sections, parametric PTFs will be developed using a neural network (NN) to estimate the parameters of the MLD model from basic soil properties. Compared to multiple linear regression, NN offers the advantage of modeling complex, nonlinear relationships between input and output variables, increasing the estimation accuracy. Furthermore, NN can continue to improve as more data become available, continuously learning and adapting to provide better estimations over various types of soils, making it a powerful tool for developing robust and reliable PTFs (Ng et al., 2020).

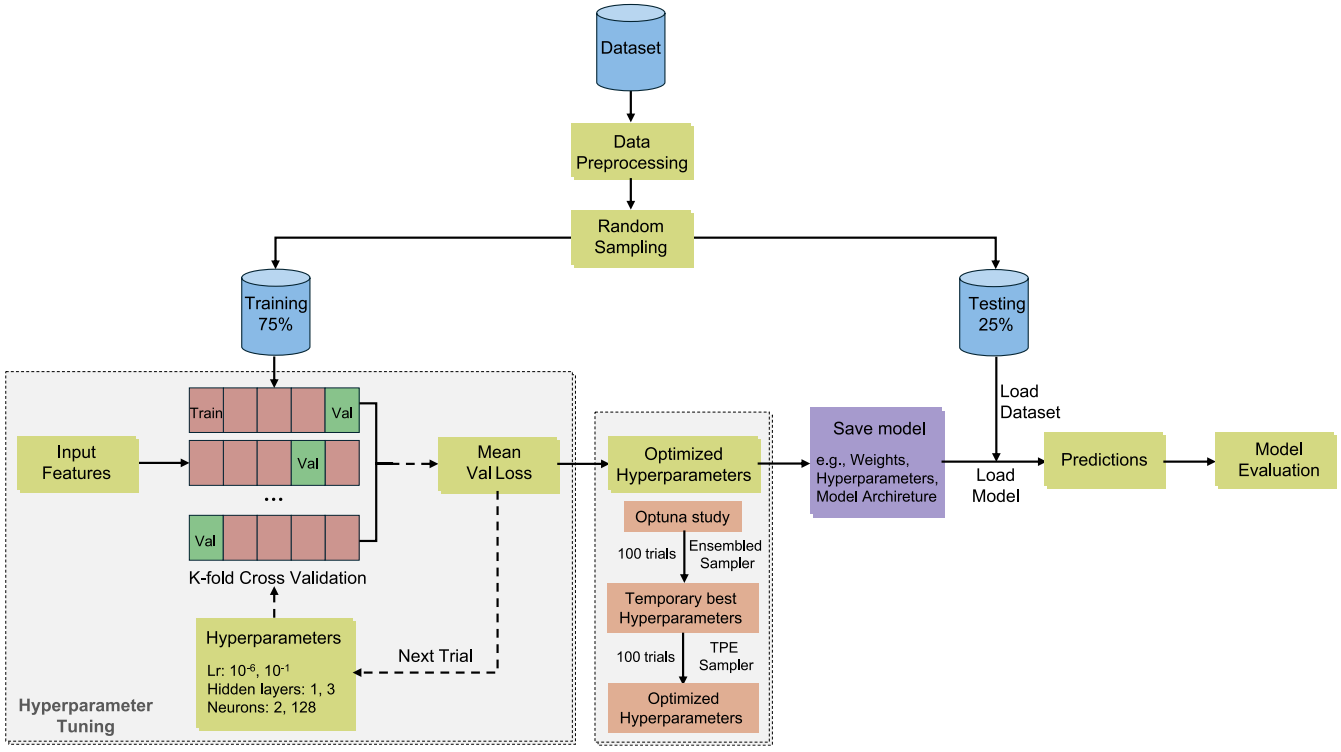

Fig. 4. Flow chart of the model building, tuning, and testing process.

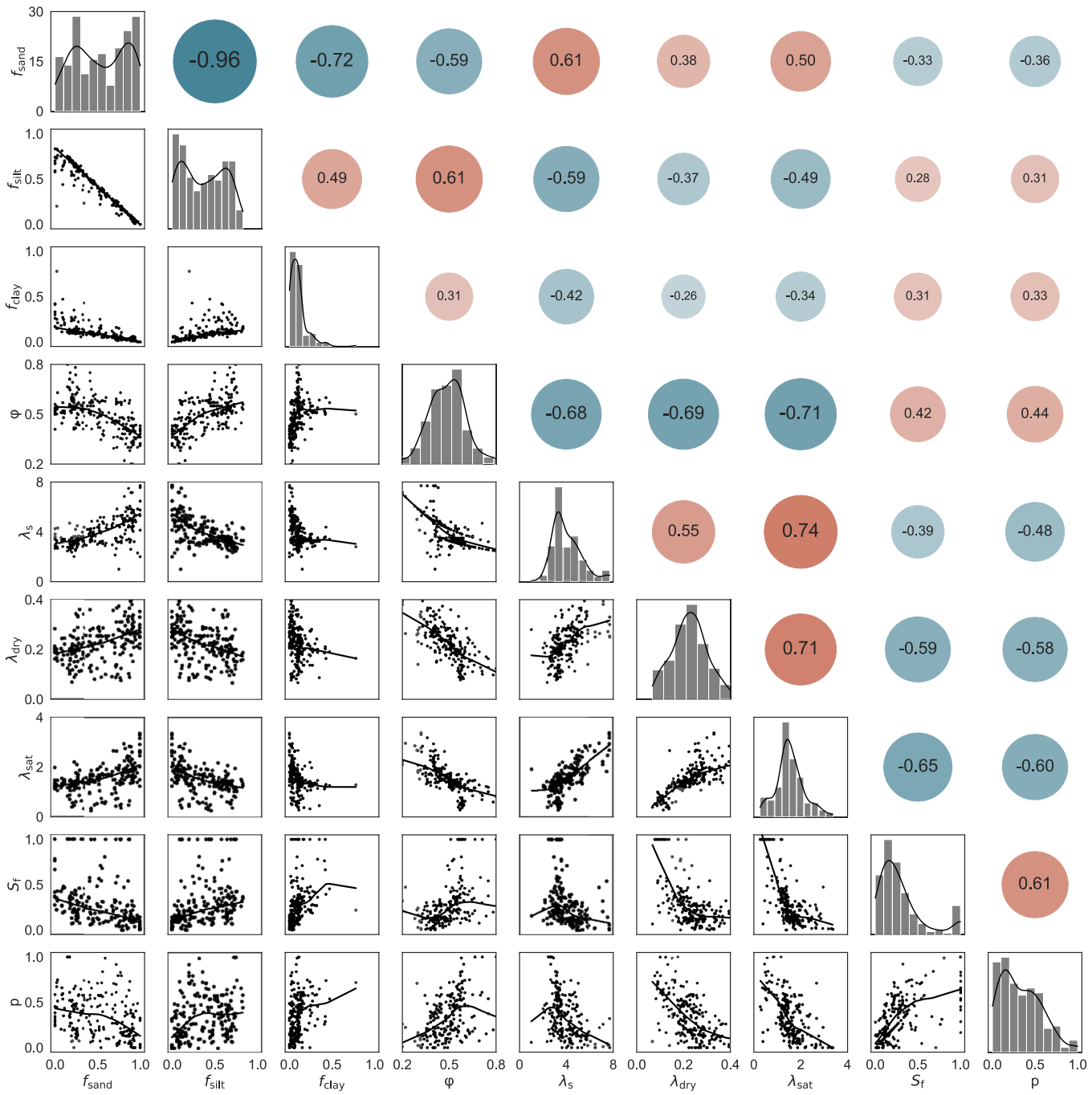

Fig. 5. The Pearson correlation matrix between predictors (f_{sand}, f_{silt}, f_{clay}, ϕ and λ_s) and parameters of Eq. [2] (λ_{sat}, λ_{dry}, S_f and p). The upper triangle shows the Pearson correlation coefficient between variables in which both the marker and number sizes are scaled proportionally to the magnitude of the correlation coefficient. The probability density distribution of each variable is given on the diagonal. The lower panel shows the scatter plots between pairs of variables.

3. Materials and methods

3.1. Dataset

To train and test the neural network to estimate MLD model parameters, a comprehensive dataset was compiled. This dataset includes 211 soils and comprises 1844 pairs of λ(S) data points, sourced from 15 different studies. These data points ensure a broad representation of λ and S values, providing robust coverage for accurate model training and testing (Fig. 2a). These studies feature diverse soil samples, such as field soils (e.g., Campbell et al., 1994; Lu et al., 2007), volcanic ash soils (e.g., McCombie et al., 2016; Tarnawski et al., 2019), and arid and semiarid soils (Zhao et al., 2018), from various locations: 104 Chinese soils, 29 American soils, 2 Italian soils, 2 German soils, 41 Canadian soils, and 33 Japanese soils (as presented in Fig. 3). Table 1 presents detailed information about the selected soil samples, in which the majority of the measurements were performed using a transient heat transfer method, with the exception of one study by Kersten (1949), which used a steady state method. The textural information for these soils is summarized in Fig. 2b. The dataset covers a wide range of soil types, including 11 out of the 12 USDA textural classes (excluding sandy clay). It predominantly includes sand, silt loam, loam, and sandy loam soils. For each selected soil, sand content (f_{sand}), silt content (f_{silt}), clay content (f_{clay}) and porosity (ϕ) are known and used in the input layer of the neural network.

Table 2
Forms and parameters of the models investigated in this study.

	Model forms		Shape parameters	References
Jo	$\frac{\lambda-\lambda_{dry}}{\lambda_{sat}-\lambda_{dry}}=\text{Alog}S+1$	$\lambda_{sat}=\lambda_s^{1-\phi}\lambda_w^{\phi}\lambda_{dry}=\frac{0.135\rho_b+0.0647}{2.7-0.947\rho_b}$	A is 0.7 for soils with $f_{clay}\leq 0.05$ and 1 soils with $f_{clay}>0.05$.	Johansen (1975)
CK	$\frac{\lambda-\lambda_{dry}}{\lambda_{sat}-\lambda_{dry}}=\frac{\kappa S}{1+(\kappa-1)S}$	$\lambda_{sat}=\lambda_s^{1-\phi}\lambda_w^{\phi}\lambda_{dry}=\chi 10^{-\eta\phi}$	κ is 3.55 for medium and fine sands and 1.90 for silty and clayey soils.The χ and η values are 0.75 and 1.20 for natural mineral soils, respectively.	Côté and Konrad (2005)
Lu	$\frac{\lambda-\lambda_{dry}}{\lambda_{sat}-\lambda_{dry}}=\exp\{\alpha[1-S^{(\alpha-\beta)}]\}$	$\lambda_{sat}=\lambda_s^{1-\phi}\lambda_w^{\phi}\lambda_{dry}=-0.56\phi+0.51$	α is 0.96 for soils with $f_{sand}\geq 0.4$ and 0.27 for soils with $f_{sand}<0.4$ and β is a suggested as 1.33.	Lu et al. (2007)
R-CK	$\frac{\lambda-\lambda_{dry}}{\lambda_{sat}-\lambda_{dry}}=\frac{\kappa S}{1+(\kappa-1)S}$	$\lambda_{sat}=\lambda_s^{1-\phi}\lambda_w^{\phi}\lambda_{dry}=\chi 10^{-\eta\phi}$	κ is 5.41, 1.64 and 2.17 for sand, soils with $f_{sand}<0.4$ and remaining soils, respectively.The χ and η values are 0.75 and 1.20 for natural mineral soils, respectively.	Fu et al. (2023a)
R-Lu	$\frac{\lambda-\lambda_{dry}}{\lambda_{sat}-\lambda_{dry}}=\exp\{\alpha[1-S^{(\alpha-\beta)}]\}$	$\lambda_{sat}=\lambda_s^{1-\phi}\lambda_w^{\phi}\lambda_{dry}=-0.56\phi+0.51$	α and β are 0.94 and 1.23 for sand, 0.59 and 1.35 for soils with $f_{sand}<0.4$, and 1.05 and 1.48 for remaining soils, respectively.	Fu et al. (2023a)

3.2. Neural network building and tuning

This section is organized into four parts. The first subsection details the steps involved in splitting and preprocessing the data for neural network training. The second subsection explores the correlation between predictors and model parameters and is followed by the feature selection. The third subsection describes the detailed architecture of the neural network. The fourth subsection outlines the procedures for optimizing the neural network's hyperparameters. All of these steps are implemented using PyTorch 2.0.1 (Paszke et al., 2019), leveraging its modules to define and execute the layers and transformations. Fig. 4 describes the flow chart of the model building, tuning and testing processes.

3.2.1. Data preprocessing

The dataset is divided into training and testing datasets with a 75–25 % split, which is implemented using the *random_split* function, with a random seed assigned to ensure consistency in the split each time it is performed. This results in a training dataset consisting of 1383 λ(S) datapoints, used to tune the neural network's hyperparameters, and a testing dataset of 461 λ(S) datapoints, used to independently test the performance of the trained model. Prior to modeling, predictors in both the training and testing datasets are standardized with the *StandardScaler* function, which computes the mean and standard deviation for each feature and uses these values to transform the data, so that each individual feature looks like standard normally distributed data, with a mean of zero and a variance of one. This leads to a fast convergence during training, improved model performance, and enhanced interpretability of the learned feature weights.

3.2.2. Feature selection

The process of choosing the optimal subset of predictors, known as feature selection, involves balancing a minimum subset of predictors with maximum prediction accuracy. It is preferable to select basic and easily measurable properties as predictors, as this ensures the established PTFs are widely applicable and can be seamlessly integrated with grid-based datasets (e.g., SoilGrids 2.0, Poggio et al. (2021)) for parameterizing soil processes in land surface models at large spatial scales. Additionally, the chosen predictors should exhibit strong correlations with the target outputs, as this allows for higher prediction accuracy with fewer predictors. In this study, we first choose f_{sand}, f_{silt}, f_{clay} as predictors due to their accessibility and previous use in PTF studies to estimate thermal, hydraulic, and biogeochemical properties (Van Looy et al., 2017). We also include ϕ to account for the influence of bulk density and particle density, of which the former is also affected by organic matter content (Minasny and McBratney, 2018) and is also one of the commonly used predictors in PTF development (Van Looy et al., 2017; Zhang and Schaap, 2017). Soil, as a three-phase mixture, includes a solid phase (λ_s) that exhibits substantially higher thermal conductivity than either water or air. Thus, λ_s is selected as the final predictor, as it is expected to greatly influence λ in both saturated and unsaturated soils (Fu et al., 2023b). Parameter λ_s can be estimated by a geometric mean model applied to quartz and other soil minerals:

$$\lambda_s=\lambda_q^{1-f_q}\lambda_o^{f_q} \tag{4}$$

where λ_q and λ_o are the thermal conductivity of quartz (7.7 W m^{-1} K^{-1}) and other soil minerals, respectively; f_q is the volume fraction of quartz in the soil solids and λ_o is taken as 2.0 W m^{-1} K^{-1} for soils with $f_q>0.2$, and 3.0 W m^{-1} K^{-1} for soils with $f_q\leq 0.2$ as suggested by Johansen (1975). However, f_q is typically measured using a combination of X-ray diffraction/X-ray fluorescence techniques, which is expensive and rarely implemented. Consequently, quartz content is not commonly known for most soils. To address this issue, Fu et al. (2023b) developed a novel DEM-GMM method to estimate λ_s from ϕ based on a combination of the differential effective medium (DEM) theory and geometric mean method (GMM), expressed as follows:

$$\left(\frac{\lambda_s}{\lambda_w}\right)^{1-\phi}=\phi^m\left(\frac{1-\lambda_s/\lambda_w}{1-(\lambda_s/\lambda_w)^{\phi}}\right)^m \tag{5}$$

where m is the effective cementation exponent, depending on the particle shape, porosity, and texture. Based on 43 soils, Fu et al. (2023b) suggested the following m values: 1.66 for soils with $f_{sand}<0.4$, 1.62 for soils with $0.4\leq f_{sand}<0.4$ and m = -1.34ϕ + 1.70 for soils with $f_{sand}=1.0$.

We further perform a Pearson correlation analysis between the selected predictors (f_{sand}, f_{silt}, f_{clay}, ϕ and λ_s) and parameters of the MLD model (λ_{sat}, λ_{dry}, S_f and p) for 212 soils. The results, depicted in Fig. 5, reveal several significant relationships. The strong negative correlation between λ_{dry} and ϕ (r = -0.69) is consistent with previous studies (Lu et al., 2007; He et al., 2017). Conversely, λ_{dry} shows a positive correlation with λ_s (r = 0.55). This positive correlation is reasonable since a dry soil, a mixture of soil solids and air, has its thermal conductivity predominantly influenced by λ_s, which is significantly higher than that of air (0.025 W m^{-1} K^{-1}). Similar correlations are observed between the predictors and λ_{sat}: there is a strong positive correlation between λ_s and λ_{sat} (r = 0.74) and a relatively large correlation between f_{sand} and λ_{sat} (r = 0.50). Both S_f and p are negatively correlated with f_{sand} (r = -0.33 and −0.36, respectively) but positively correlated with f_{clay} (r = 0.31 and 0.33, respectively). This aligns with the results in Fig. 1, where the λ(S) curves show a more pronounced 'flat tail' with increasing S_f and p, typical characteristics of fine-textured soils.

3.2.3. Neural network architecture

The neural network architecture used in this study is a multi-layer perceptron designed for regression tasks with specific constraints on

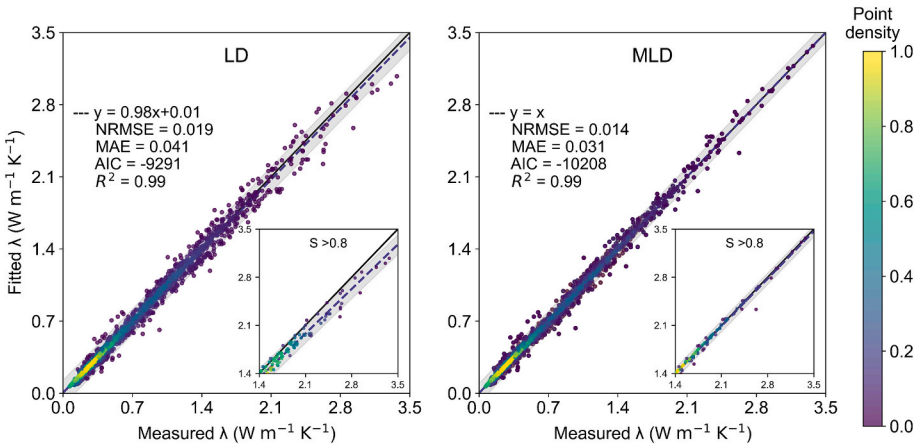

Fig. 6. Comparison of fitted LD and MLD model soil thermal conductivity (λ) values versus measured λ values for soils in the complete dataset. The insets show λ values in the saturation S range greater than 0.8. The solid lines, the dashed lines and the gray region are the 1:1 line, the regression lines and 95% prediction interval.

the output. It begins with an input layer that takes in features of dimension 5: f_{sand}, f_{silt}, f_{clay}, ϕ and λ_s. The hidden layers are fully connected and use ReLU activation functions followed by dropout layers with a dropout probability of 0.2 to prevent overfitting. The final layer outputs four values, which are subsequently transformed using sigmoid activation to ensure they lie within the range [0, 1]. These outputs are then scaled and shifted with the *torch.matmul* function, resulting in the final outputs meeting specific constraints: $0.01 \leq S_f \leq 0.95$; $0.01 \leq p \leq 0.95$; $0.07 \leq \lambda_{dry} \leq 0.35$; $0.27 \leq \lambda_{sat} \leq 3.37$. During the training loop, the neural network is initialized with the Adam optimizer and a learning rate scheduler, StepLR, is set up to reduce the learning rate by a factor of 0.2 every 50 epochs, which helps in fine-tuning the learning process over time.

3.2.4. Hyperparameter tuning

Hyperparameter tuning is crucial to optimize the performance of the neural network. The hyperparameters being tuned include the learning rate, the number of hidden layers, and the number of neurons in each hidden layer. The learning rate is sampled from a log-uniform distribution within the range $[10^{-6}, 10^{-1}]$, allowing for the exploration of a wide range of potential learning rates. The number of hidden layers is an integer of 1, 2, or 3, while the number of neurons in each hidden layer is sampled from an integer uniform distribution of 2 to 128.

In this study, we employ Optuna (Akiba et al., 2019), a powerful hyperparameter optimization framework, to identify the optimal set of hyperparameters for the neural network. Different methods have been developed to efficiently search for the best combination of hyperparameters, such as grid search, random search and Bayesian optimization. Because grid search does not apply to continuous values like learning rate, we design a two-step sampling strategy to leverage the strengths of two sampling methods: Tree-structured Parzen Estimator (TPE) Sampler based on Bayesian optimization and Random Sampler based on random search. In the first 100 trials, we combine these two methods into an ensemble sampler and use it in a randomized manner. For the subsequent 100 trials, we exclusively use the TPE Sampler. This approach benefits from the exploration capabilities of the Random Sampler in the early stages while utilizing the TPE Sampler's more refined search capabilities in the latter stages to fine-tune and optimize the results. More details about this ensemble sampler can be found in section 4.2.

The tuning process uses K-Fold cross-validation with five splits to ensure the model's robustness and generalization capability. In each fold, one subset serves as the validation dataset while the remaining four subsets are used for training. During each trial, the neural network model is initialized with the suggested hyperparameters, and the model undergoes training for a maximum of 5000 epochs with early stopping implemented to halt training if no improvement is observed over 300 consecutive epochs (Prechelt, 1998). The validation losses across five folds are averaged to determine the trial's performance. The loss is computed as the Smooth L1 loss (also known as Huber loss):

$$\text{Smooth L1 loss} = \frac{1}{N}\sum_{i=1}^{N} L\left(\lambda^i, \widehat{\lambda}^i\right) \tag{6}$$

where N is the number of data points, and λ and $\widehat{\lambda}_i$ are the measured and modeled estimates at the i_{th} data point, respectively. $L\left(\lambda^i, \widehat{\lambda}^i\right)$ is defined as:

$$L\left(\lambda^i, \widehat{\lambda}^i\right) = \begin{cases} 0.5\left(\lambda^i - \widehat{\lambda}^i\right)^2 & \text{if } \left|\lambda^i - \widehat{\lambda}^i\right| < 1 \\ \left|\lambda^i - \widehat{\lambda}^i\right| - 0.5 & \text{otherwise} \end{cases} \tag{7}$$

The Smooth L1 loss function offers several advantages over the commonly used Mean Square Error (MSE) loss function. In contrast to MSE that emphasizes large errors due to its quadratic nature, the Smooth L1 loss transitions to a linear behavior for large errors, reducing the impact of outliers on the overall loss, making it more stable and less sensitive to anomalies in the data. Additionally, for small errors, the Smooth L1 loss behaves similarly to MSE, maintaining the benefit of smooth optimization.

After the completion of all 200 trials, the best model, characterized by the lowest average validation loss, is saved, alongside the hyperparameter settings and the model's weights that produced it. This ensures that the exact state of the best performing model can be retrieved for future use without needing to retrain it from scratch.

3.3. Comparison with other λ(S) models

To rigorously assess the performance of the modified Lu and Dong model (MLD), we perform a comparative analysis against five established models, including the Johansen (1975) model (J75), the Côté and Konrad (2005) model (CK05), the Lu et al. (2007) model (L07), and recalibrated versions of the CK05 (R-CK05) and L07 (R-L07) models. Fu et al. (2023a) used a more extensive calibration dataset to refine CK05 and L07 models, proposing alternate empirical values for shape parameters in their forms. A noteworthy limitation in both the J75 and CK05 models lies in the ambiguous boundary between the categories of "medium and fine sands" and "silty and clayey soils." This absence of explicit boundary definitions can result in an incorrect selection of the λ(S) relationship. To mitigate this issue, we employ classifications based on coarse-textured soils ($f_{sand} \geq 0.4$) and fine-textured soils ($f_{sand} < 0.4$),

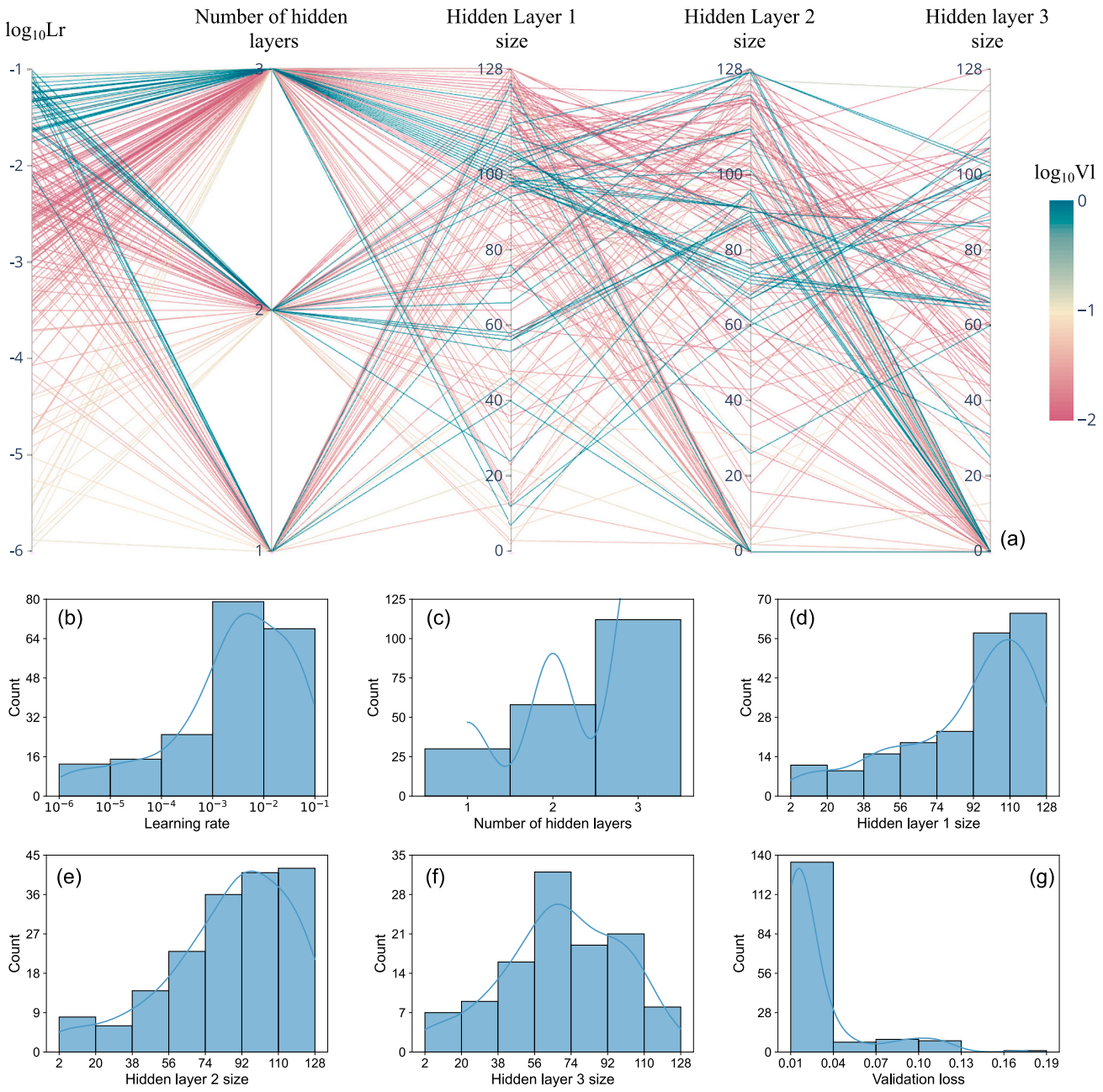

Fig. 7. (a) Hyperparameter tuning results for 200 trials with Optuna, and Lr and Vl are learning rate and validation loss, respectively. (b)-(g) Histograms of the hyperparameters during the training.

as suggested by Lu et al. (2007), to represent "medium and fine sands" and "silty and clayey soils" in the J75 and CK05 models, respectively. Detailed forms and shape parameters of these models are provided in Table 2.

3.4. Model assessment

In this study, we compare λ estimates with different models ($\widehat{\lambda}^{(i)}$) to directly measured λ values ($\lambda^{(i)}$). The model performances are evaluated using four metrics: normalized root mean square error (NRMSE), mean absolute error (MAE), Akaike's information criterion (AIC) and the coefficient of determination (R^2):

$$\mathrm{NRMSE} = \frac{1}{\lambda^i_{max} - \lambda^i_{min}} \sqrt{\frac{\sum_{i=1}^{N} \left(\lambda^i - \widehat{\lambda}^i\right)^2}{N}} \tag{8}$$

$$\mathrm{MAE} = \sqrt{\frac{\sum_{i=1}^{N} \left|\lambda^i - \widehat{\lambda}^i\right|}{N}} \tag{9}$$

$$\mathrm{AIC} = N \ln\left(\frac{\sum_{i=1}^{N} \left(\lambda^i - \widehat{\lambda}^i\right)^2}{N}\right) + 2p \tag{10}$$

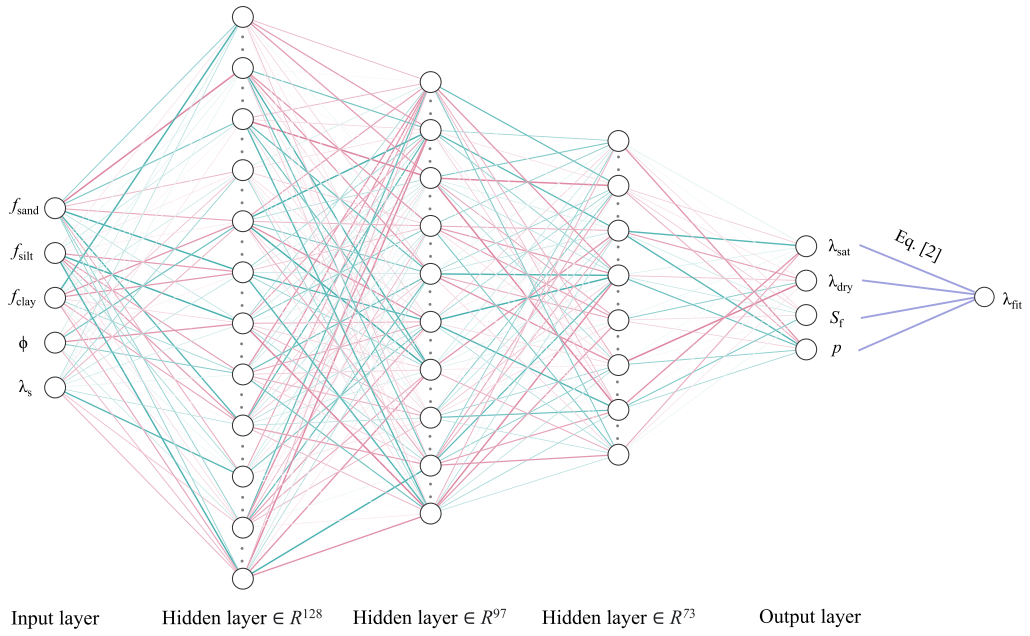

Fig. 8. Neural network architecture with optimized hyperparameters. Red and green colors indicate positive and negative weights for each neuron, respectively, for better visualization purposes. Note that these colors do not represent the actual weights.

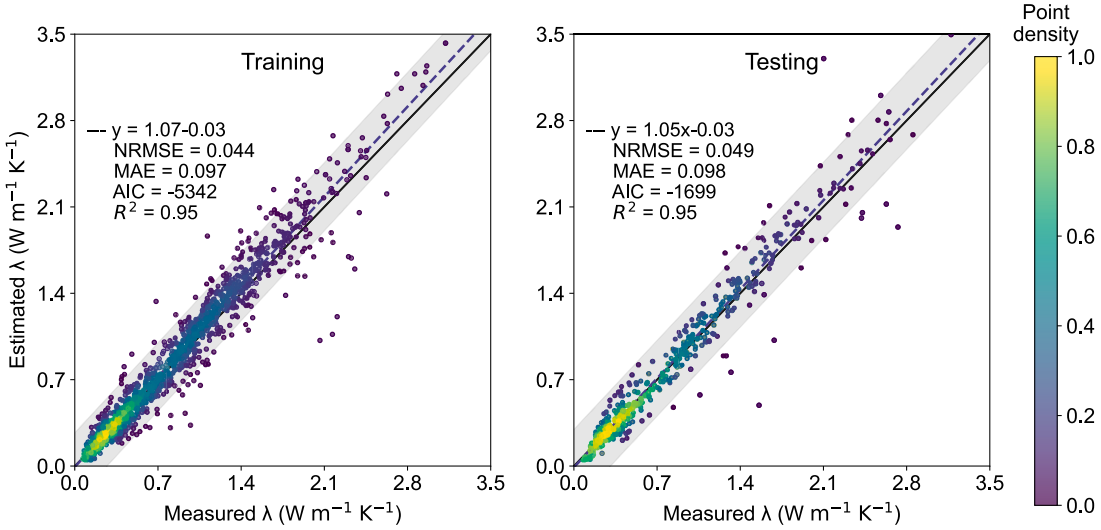

Fig. 9. Comparison of soil thermal conductivity (λ) values estimated with the NN-MLD model versus measured λ values for the training dataset and the testing dataset. The solid lines, the dashed lines and the gray region are the 1:1 line, the regression lines and the 95% prediction interval.

$$R^2 = 1 - \frac{\sum_{i=1}^{N}\left(\lambda^i - \widehat{\lambda}^i\right)^2}{\sum_{i=1}^{N}\left(\lambda^i - \frac{1}{N}\widehat{\lambda}^i\right)^2} \tag{11}$$

4. Results and Discussion

4.1. Fitting the MLD model to λ(S) observations

Fig. 6 compares the LD and MLD model fitted λ values versus the measured λ values for the whole dataset. Overall, compared to the LD model, measured and fitted values by the MLD model distribute more closely along the 1:1 line, the slope of the regression line is closer to one, and the intercept is closer to zero. Error analysis also shows that compared to the measured values, the NRMSE, MAE, AIC and R^2 values of the fitted results by the MLD model are 0.014, 0.031 W m^{-1} K^{-1}, −10208 and 0.99, respectively and the corresponding values of the LD model are 0.019, 0.041 W m^{-1} K^{-1}, −9291 and 0.99, respectively. Except for R^2, all metrics indicate that the MLD model performs better than the LD model. The improved performance of the MLD model is particularly evident in the capillary regime, where the data fitted by the LD model are much more scattered, as shown in the inset in Fig. 6. In the

Table 3
NRMSE, MAE, r and R^2 for the MLD model parameters (S_f, p, λ_{dry} and λ_{sat}) comparing fitted and predicted values using the trained neural network.

	NRMSE	MAE	r	R^2
S_f	0.183	0.102	0.77	0.59
p	0.248	0.187	0.17	0.03
λ_{dry}	0.114	0.041	0.77	0.59
λ_{sat}	0.074	0.171	0.94	0.88

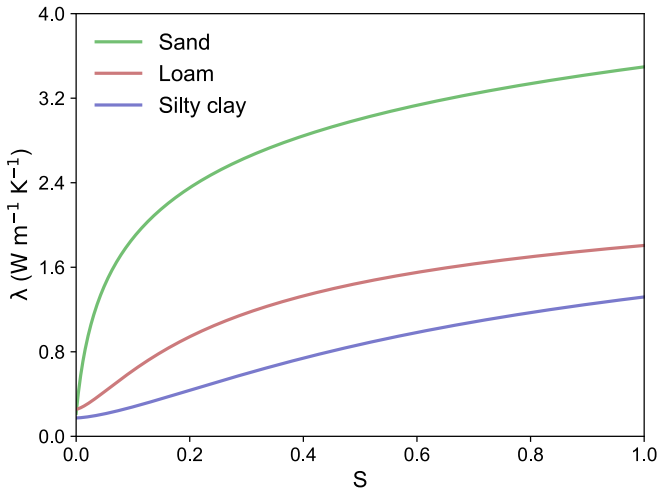

Fig. 10. Fitted NN-MLD model thermal conductivity (λ) versus degree of saturation (*S*) curves for three representative soils with distinct textures.

near saturation range ($S > 0.8$), the NRMSEs for λ are 0.036 for the LD model and 0.013 for the MLD model; the MAEs are 0.085 and 0.020 W m^{-1} K^{-1}, respectively; the AICs are −794.0 and −1161.0, respectively; and R^2 values are 0.99 and 1.00, respectively. Error analysis near saturation indicates that the MLD model performs consistently well across the full range of saturation levels, in contrast to the LD model, which shows poor performance near saturation.

4.2. Determination of optimized hyperparameters

This study uses Optuna for hyperparameter optimization, which automates the process of exploring hyperparameter spaces within the suggested range to find the optimal configuration to minimize the average validation loss. In this Optuna study, we initially use a custom ensemble sampler that integrates two different samplers: TPE Sampler and Random Sampler. This method leverages the strengths of both sampling strategies during the first 100 trials, aiming to balance exploitation and exploration in the optimization process. After the initial 100 trials, a set of provisional hyperparameters is identified. These provisional values are then used as initial values for further exploration via the *study.enqueue_trial* function. The study continues with another 100 trials, now using only the TPE Sampler to refine and optimize the hyperparameters. The results in Fig. 7 support the effectiveness of this strategy, where the tuning process explores the search space broadly for all hyperparameters, while emphasizing specific ranges, such as a learning rate between 10^{-2} and 10^{-3} (Fig. 7b), three hidden layers (Fig. 7c), the number of neurons in hidden layer 1 between 92 and 128 (Fig. 7d), the number of neurons in hidden layer 2 between 92 and 128 (Fig. 7e), and the number of neurons in hidden layer 3 between 56 and 74 (Fig. 7f). This broad exploration can be attributed to the Random Sampler, which is useful to cover the search space comprehensively. Most trials are centered on learning rates between 10^{-2} and 10^{-3}, because the TPE Sampler focuses on regions of the hyperparameter space that yielded good results in the past to suggest new hyperparameters (Fig. 7a and 7 g).

After the completion of all 200 trials, results demonstrate that the network with a learning rate of 2.62×10^{-3}, 128 neurons in hidden layer 1, 97 neurons in hidden layer 2, and 73 neurons in hidden layer 3 converges to the lowest smooth L1 loss. Subsequently, the model architecture with the optimized hyperparameters is saved as the final trained model, named the NN-MLD model, which is illustrated in Fig. 8.

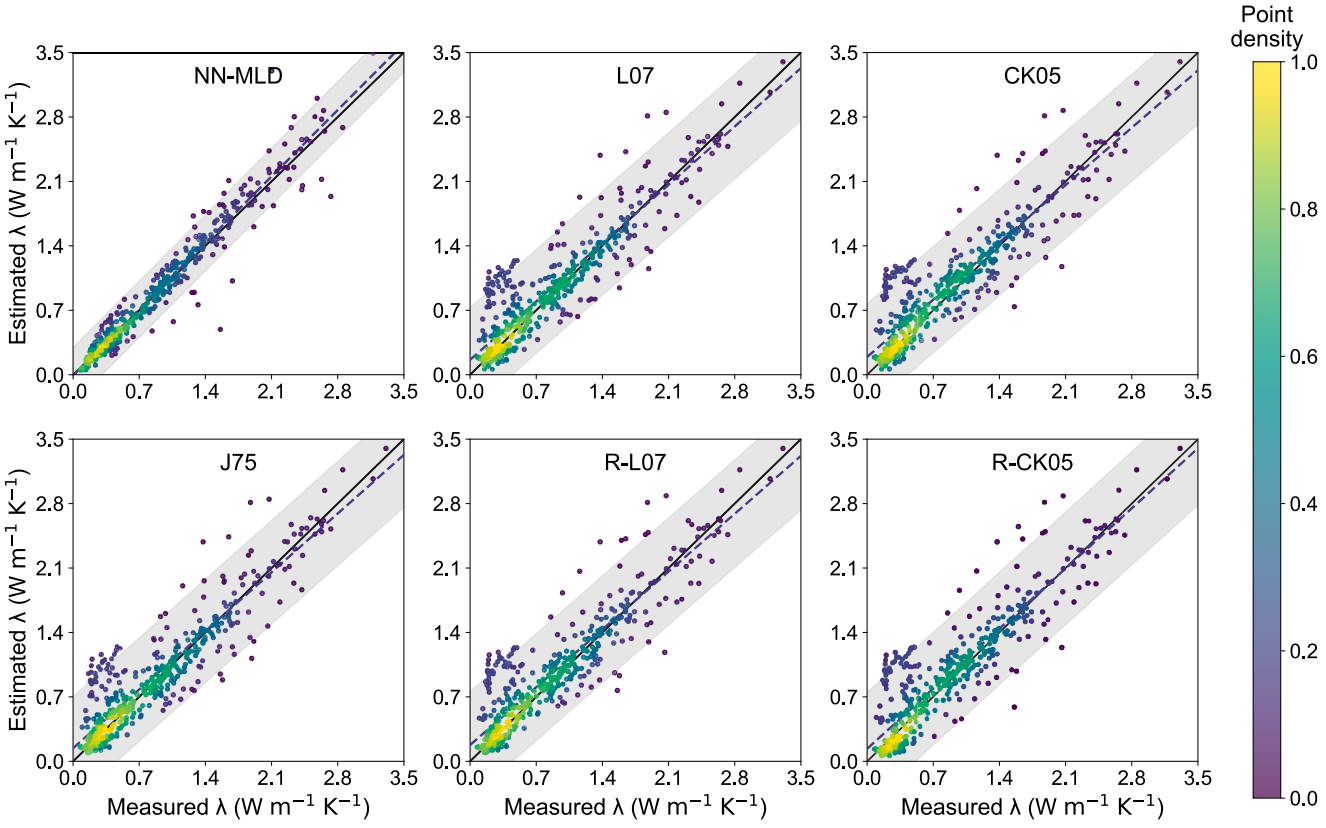

Fig. 11. Comparison of soil thermal conductivity (λ) estimated with the NN-MLD model as well as five pre-existing models versus measured λ values for the testing dataset. The solid lines, the dashed lines and the gray region are the 1:1 line, the regression lines and the 95% prediction interval.

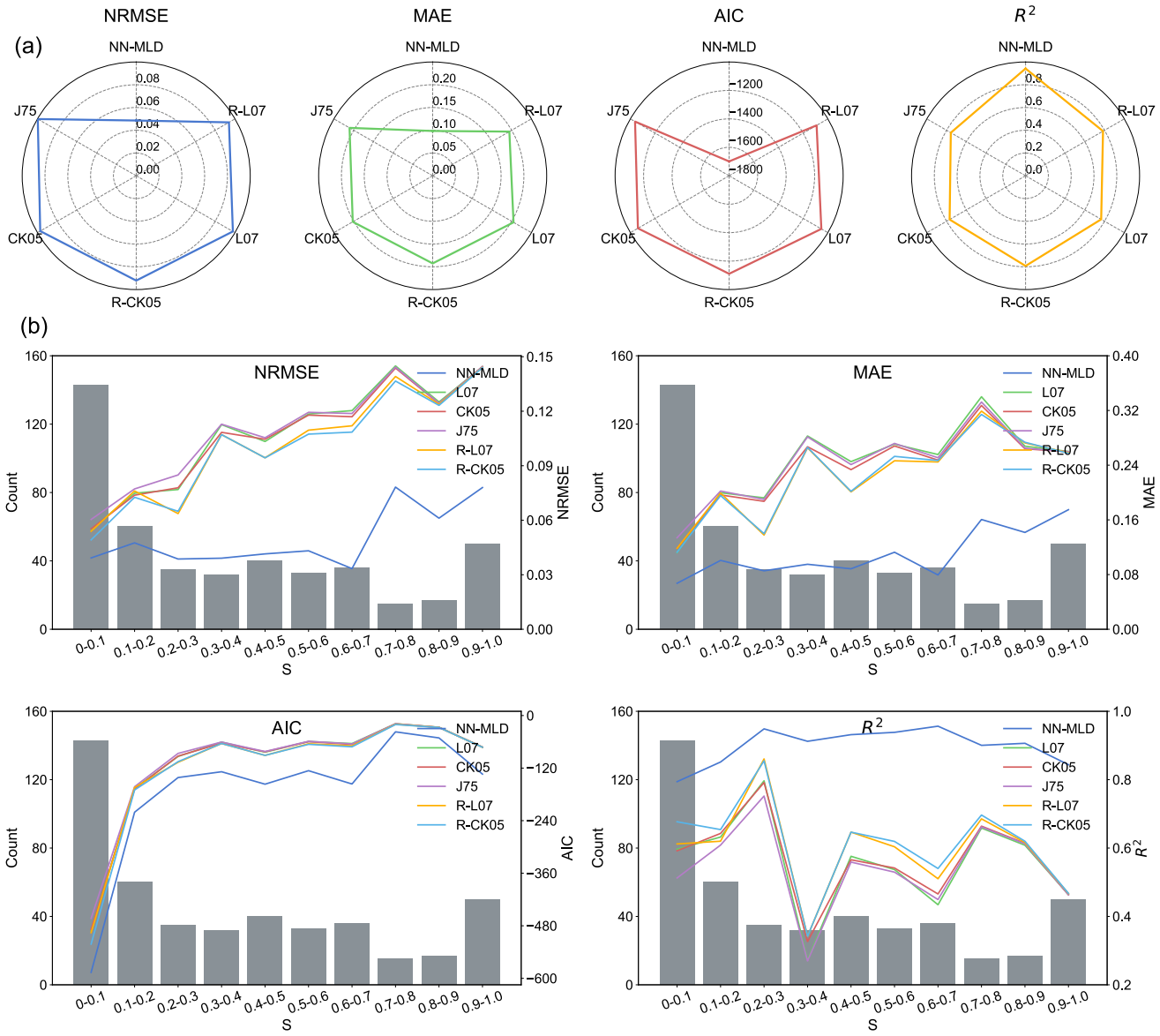

Fig. 12. (a) NRMSE, MAE, AIC and R^2 values of six models for the testing dataset; (b) NRMSE, MAE, AIC and R^2 variations for ten saturation *S* classes.

4.3. Estimating the MLD model parameters

The MLD parameters, represented by the four neurons in the output layer, are predicted using the predictors in the input layer with the NN-MLD model, as shown in Fig. 9. Table 3 presents the NRMSE, MAE, r and R^2 for the directly fitted parameters and the estimated parameters of the MLD model: λ_{sat}, λ_{dry}, S_f and p. The NN-MLD model accurately estimates λ_{sat} with an NRMSE of 0.074, MAE of 0.171 W m^{-1} K^{-1}, r of 0.94 and R^2 of 0.85. This high accuracy is due to the inclusion of λ_s and ϕ as inputs, which are highly correlated with λ_{sat}, as illustrated in Fig. 5. Because saturated soils can be regarded as a mixture of soil solids and water, it is unsurprising that λ_s and ϕ are essential inputs to compute λ_{sat}. Additionally, the NN-MLD model produces satisfactory results for λ_{dry} and S_f as shown in Table 3, with NRMSE values of 0.114 and 0.183, MAE values of 0.041 W m^{-1} K^{-1} and 0.102, r values of 0.77, R^2 values of 0.59 for λ_{dry} and S_f, respectively. The lowest agreement between fitted and estimated parameters occurs for parameter p, indicating a high uncertainty. The predicted p values with the NN-MLD model have a limited range: the median is 0.30 with a standard deviation (SD) of 0.09. In contrast, directly fitting the MLD model to data results in p values with a median of 0.37 and a much larger SD of 0.23. However, this does not necessarily mean that the NN-MLD model cannot make accurate estimations. As parameters of the MLD model are correlated (Fig. 5), they should not be assessed individually for the overall performance. Instead, a holistic evaluation considering the interactions and combined estimation power of all parameters provides a more accurate assessment of the model's efficacy (see section 4.4).

4.4. Model evaluation

Fig. 9 presents the performance of the NN-MLD model on the training and testing dataset. Overall, the developed model provides accurate estimates for both datasets, with NRMSEs of 0.044 and 0.049, MAEs of 0.097 and 0.098 W m^{-1} K^{-1}, AICs of −5342 and −1699, and R^2 of 0.95. The slightly better performance on the training dataset is unsurprising, as the training process is designed to minimize the smooth L1 loss on the training dataset. More importantly, the close performance of the model on both training and testing datasets can be attributed to the procedures implemented to prevent overfitting during the training process, including k-fold cross validation, early stopping and dropout. It is noteworthy that for both datasets, the NN-MLD model shows a slight overestimation at high λ values. This arises from the errors in estimating

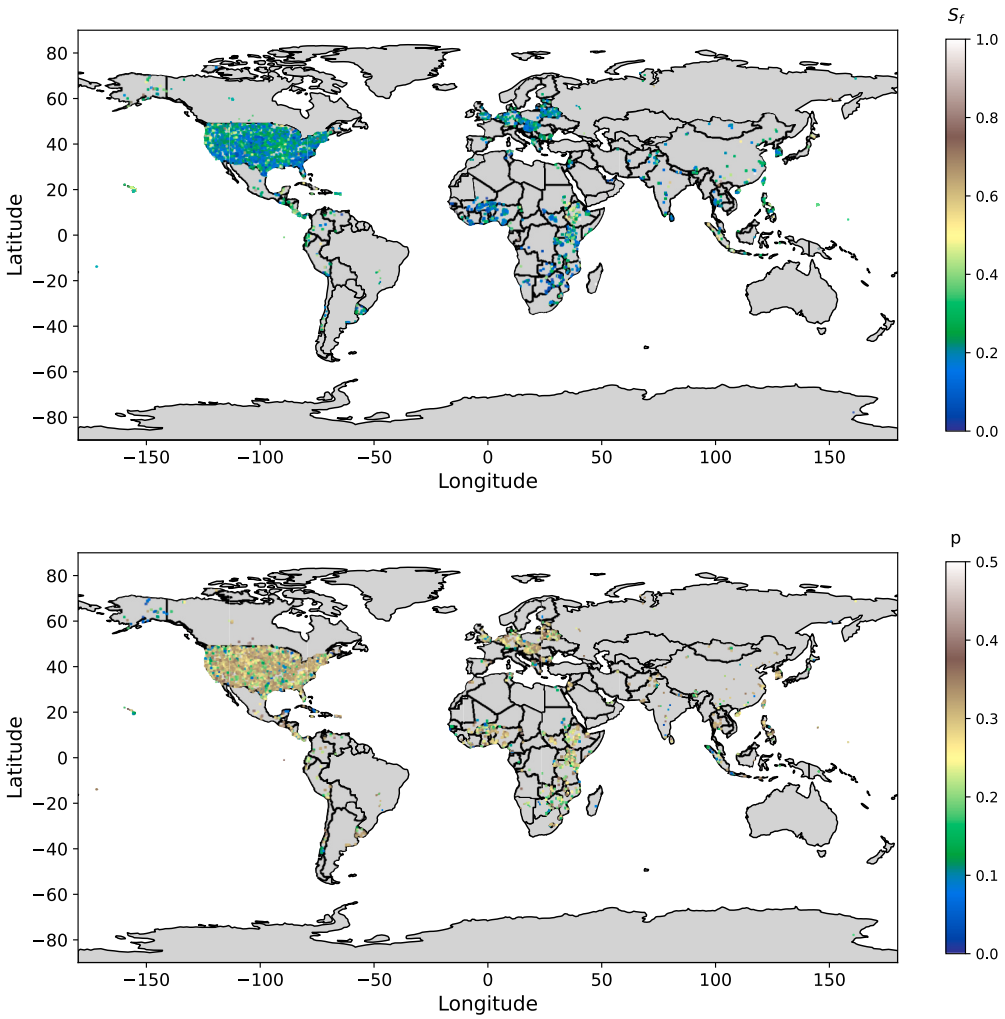

Fig. 13. The S_f and p maps estimated with the NN-MLD model using the data points at surficial horizon within WoSIS Soil Profile Database.

the predictor λ_s with the DEM-GMM method (Eq. [5]), which combines the differential effective medium theory and geometric mean method. The differential effective medium theory assumes zero grain contact, which is particularly problematic for soils with low porosity. This is especially relevant for semi-arid soils, such as those from Zhao et al. (2018), which have ϕ values as low as 0.2.

Fig. 10 shows estimated $\lambda(S)$ curves with the NN-MLD model for three representative soils: Stable Island sand with 100 % sand and 100 % quartz from Tarnawski et al. (2015), E01 loam with 45 % sand and 9 % clay from Zhao et al. (2018), and FS#1 silty clay with 0 % sand, 42 % clay and 21 % quartz from Tarnawski et al. (2015). These soils represent sand, loam, and silty clay, with porosities of 0.36, 0.55 and 0.51. The estimated λ_{sat} and λ_{dry} values are 3.497 and 0.217 W m^{-1} K^{-1} for sand, 1.806 and 0.256 W m^{-1} K^{-1} for loam, and 1.319 and 0.174 W m^{-1} K^{-1} for silty clay, respectively. The S_f and p values are also calculated from predictors, yielding $S_f = 0.013$, 0.138 and 0.410, and $p = 0.025$, 0.289 and 0.332 for sand, loam, and silty clay, respectively. The three estimated $\lambda(S)$ curves show typical characteristics: within the hydration regime, the $\lambda(S)$ curve of the silty clay soil has the most pronounced 'flat tail', behaving like fine-textured soils. The $\lambda(S)$ curve of the sand soil shows the most drastic increase in the pendular regime and the largest magnitude of λ over the entire S range, typical of coarse soils. As S approaches 1, all three curves converge to $\lambda = \lambda_{sat}$, indicating that the MLD model (Eq. [2]) effectively overcomes the limitation of the LD model near saturation.

4.5. Comparison with pre-existing $\lambda(S)$ models

We perform a comparative analysis of the NN-MLD model with five pre-existing $\lambda(S)$ models (i.e., three model types, with two of them subject to two types of calibration) using the testing dataset. The results presented in Fig. 11 demonstrate that the NN-MLD model stands out as the only model providing reliable estimates, with observed and estimated values closely aligned. In contrast, the other models exhibit significant scatter, deviating from the 1:1 line, and they show a clear tendency to overestimate λ in the lower λ range (< 0.7 W m^{-1} K^{-1}). Fig. 12 presents the four error metrics for these models to estimate λ. Among the evaluated models, the NN-MLD model demonstrates superior performance across all four metrics: it achieves the lowest NRMSE of 0.049, the lowest MAE of 0.098 W m^{-1} K^{-1}, the lowest AIC score of -1699, and the highest R^2 of 0.94. In comparison, the other models yield NRMSEs ranging from 0.092 to 0.100, MAEs ranging from 0.193 to 0.210 W m^{-1} K^{-1}, AICs scores ranging from -1111 to -1038, and R^2 values from 0.76 to 0.78. These results indicate that the NN-MLD model developed in this study is the most accurate and reliable model among those assessed.

Fig. 12 also shows the error metrics obtained for six models across ten S classes, detailing the error analysis results for each class. The results clearly demonstrate that the NN-MLD model substantially outperforms the pre-existing models across all S ranges. This improved performance is particularly evident in the intermediate S range. For example, for S values ranging from 0.6 to 0.7, the NN-MLD model has a

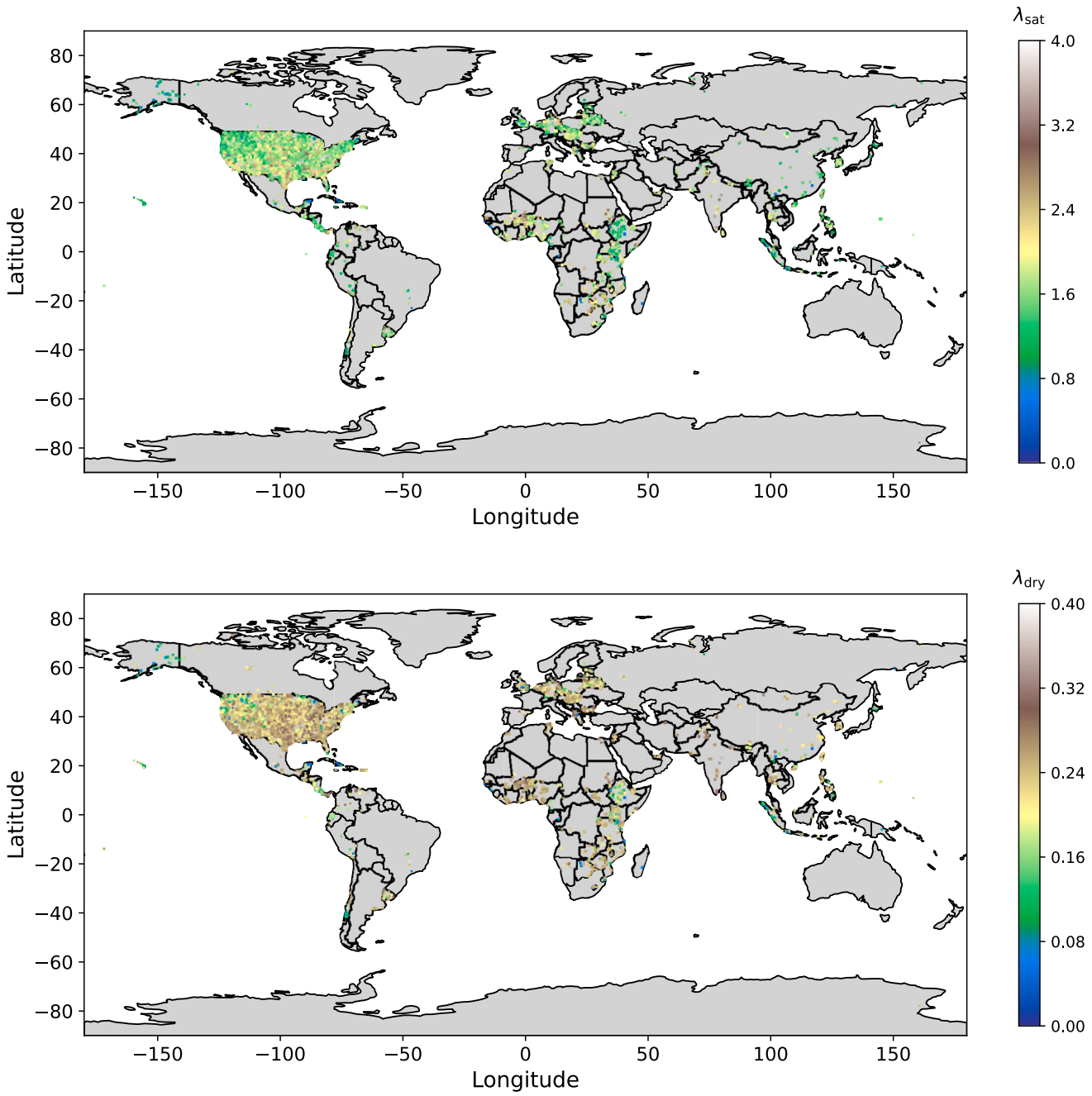

Fig. 14. The λ_{sat} and λ_{dry} maps estimated with the NN-MLD model using the data points at surficial horizon within WoSIS Soil Profile Database.

NRMSE of 0.033 and an MAE of 0.079 W m^{-1} K^{-1}. In contrast, the other models exhibit limited accuracy with NRMSEs ranging from 0.108 to 0.120 and MAEs ranging from 0.245 to 0.256 W m^{-1} K^{-1}, which are approximately three times larger than those of the NN-MLD model. Additionally, for S values from 0.3 to 0.4, the NN-MLD model attains a much higher R^2 value of 0.91, compared to R^2 values of only 0.27 to 0.34 for the other models. Our analysis shows that the performances of the R-L07 and R-CK05 models rank in second and third place for most S ranges. In comparison, the original versions of the J75, CK05, and L07 models demonstrate inferior performances based on the four metrics considered.

In recent years, there has been significant progress in applying neural networks to estimate the values of soil λ (Zhang et al., 2020a; Zhang et al., 2020b; Li et al., 2022). However, a key limitation in these studies is the lack of publicly available raw codes for implementing these models, which has hindered direct comparisons against them both within this study and with others in the field. To address this gap, we have made both the dataset used in this study and the trained NN-MLD model publicly accessible through Mendeley Data (Fu, 2024), allowing future researchers to replicate the results and facilitate comparisons more easily.

5. Conclusions and outlook

In this study, we first develop the MLD model which accurately describes λ(S) data across the full range of saturation levels. The NN model is then used to establish PTFs to estimate the MLD model parameters (λ_{sat}, λ_{dry}, S_f and p) using soil basic properties. The hyperparameters of the NN model are tuned with Optuna using a calibration dataset, and the final model architecture, incorporating the optimized hyperparameters,

is identified and saved as the NN-MLD model. Evaluation on an independent testing dataset shows that, compared to pre-existing models, the new NN-MLD model is the best model to describe the $\lambda(S)$ relationship accurately over the entire range of saturation for various types of soils. The NN-MLD model is implemented in Python code under an open-source license which can be found in Supplementary Material. It can make thermal property estimations for a variety of scenarios and scales. An example using soil properties from the WoSIS Soil Profile Database by Batjes et al. (2024) as inputs into the NN-MLD model to generate a global distribution of parameters λ_{sat}, λ_{dry}, S_f and p is also presented (Figs. 13 and 14). This highlights the potential of the NN-MLD model to be incorporated into land surface models, enabling the description and parameterization of soil processes at large spatial scales.

While the NN-MLD model shows promising performance, several potential improvements and avenues for future research remain. First, the established PTF (NN-MLD) is primarily based on mineral and repacked soils, which may limit its applicability to organic and well-structured soils. Organic soils, such as peat, and undisturbed soils with microaggregated structures can exhibit significantly different thermal properties due to their unique composition and structure (Abu-Hamdeh and Reeder, 2000; Zhao et al., 2019; Schjønning, 2021). These differences will inevitably affect the fitted MLD model parameters, potentially challenging the validity of the NN-MLD model. Therefore, a more comprehensive database should further increase the capabilities of the established PTF. Second, predictors for the PTF should be both spatially specific and easily identifiable, requiring minimal time and experimental effort while still providing relevant information. To capture soil diversity and spatial heterogeneity, environmental variables such as topography, climate, and land cover must be integrated into the development of PTFs, particularly when considering global model applications (Van Looy et al., 2017). Finally, since both θ and ϕ, which significantly influence λ, can vary over time due to factors such as soil wetting- drying cycles, freezing-thawing cycles, or land management practices, developing a temporal PTF would be a valuable next step (Vereecken et al., 2022). This could allow the model to account for the dynamic nature of soil properties and improve its capabilities for time-varying scenarios.

CRediT authorship contribution statement

Yongwei Fu: Writing – original draft, Visualization, Validation, Methodology, Funding acquisition, Data curation, Conceptualization. **Robert Horton:** Writing – review & editing, Validation, Funding acquisition, Conceptualization. **Joshua Heitman:** Writing – review & editing, Validation, Supervision, Funding acquisition, Conceptualization.

Declaration of competing interest

The authors declare that they have no known competing financial interests or personal relationships that could have appeared to influence the work reported in this paper.

Acknowledgements

This research was supported by the National Natural Science Foundation of China (Grant Number: 42407414), US National Science Foundation (Grant Number: 2037504) and USDA-NIFA Multi-State Projects 4188 and 5188.

Appendix A. Supplementary data

Supplementary data to this article can be found online at https://doi.org/10.1016/j.compag.2025.110321.

Data availability

Data will be made available on request.

References

Abu-Hamdeh, N.H., Reeder, R.C., 2000. Soil thermal conductivity effects of density, moisture, salt concentration, and organic matter. Soil. Sci. Soc. Am. J. 64, 1285–1290. https://doi.org/10.2136/sssaj2000.6441285x.

Akiba, T., Sano, S., Yanase, T., Ohta, T., Koyama, M., 2019. Optuna: A next-generation hyperparameter optimization framework. Proc. ACM. SIGKDD. Int. Conf. Knowl. Discov. Data. Min 2623–2631. https://doi.org/10.1145/3292500.3330701.

Al-Shammary, A.A.G., Caballero-Calvo, A., Jebur, H.A., Khalbas, M.I., Fernández-Gálvez, J., 2022. A novel heat-pulse probe for measuring soil thermal conductivity: Field test under different tillage practices. Comput. Electron. Agric. 202, 107414. https://doi.org/10.1016/j.compag.2022.107414.

Batjes, N.H., Calisto, L., de Sousa, L.M., 2024. Providing quality-assessed and standardised soil data to support global mapping and modelling (WoSIS snapshot 2023). Earth. Syst. Sci. Data 16, 4735–4765. https://doi.org/10.5194/essd-16-4735-2024.

Campbell, G.S., Jungbauer, J.D., Bidlake, W.R., Hungerford, R.D., 1994. Predicting the effect of temperature on soil thermal conductivity. Soil. Sci 158, 307–313. https://doi.org/10.1097/00010694-199411000-00001.

Fu, Y., Lu, S., Ren, T., Horton, R., Heitman, J.L., 2021. Estimating soil water retention curves from soil thermal conductivity measurements. J. Hydrol 127171. https://doi.org/10.1016/j.jhydrol.2021.127171.

Fu, Y., Ghanbarian, B., Horton, R., Heitman, J., 2023a. Robust calibration and evaluation of a percolation-based effective-medium approximation model for thermal conductivity of unsaturated soils. Geoderma 438, 116631. https://doi.org/10.1016/j.geoderma.2023.116631.

Fu, Y., Jones, S., Horton, R., Heitman, J., 2023b. Excluding quartz content from the estimation of saturated soil thermal conductivity: Combined use of differential effective medium theory and geometric mean method. Agric. for. Meteorol. 342, 109743. https://doi.org/10.1016/j.agrformet.2023.109743.

Fu, Y., 2024. Neural Network for Predicting Soil Thermal Conductivity. Mendeley. Data V3. https://doi.org/10.17632/by2xmg7jvc.3.

Haigh, S.K., 2015. Thermal conductivity of sands. Géotechnique 62, 617–625. https://doi.org/10.1680/geot.11.p.043.

Hailemariam, H., Shrestha, D., Wuttke, F., Wagner, N., 2017. Thermal and dielectric behaviour of fine-grained soils. Environ. Geotech. 4, 79–93. https://doi.org/10.1680/jenge.15.00042.

He, H., Zhao, Y., Dyck, M.F., Si, B., Jin, H., Lv, J., Wang, J., 2017. A modified normalized model for predicting effective soil thermal conductivity. Acta. Geotech 12, 1281–1300. https://doi.org/10.1007/s11440-017-0563-z.

Hopmans, J.W., Dane, J.H., 1986. Thermal conductivity of two porous media as a function of water content, temperature, and density. Soil. Sci 142, 187–195. https://doi.org/10.1097/00010694-198610000-00001.

Jalali, S.A.S., Navidi, M.N., Mohammadi, J.S., Meymand, A.Z., Esmail, Z.M., 2019. Prediction of soil cation exchange capacity using different soil parameters by intelligent models. commun. Soil. Sci. Plant. Anal. 50, 2123–2139. https://doi.org/10.1080/00103624.2019.1654501.

Johansen, O. 1975. Thermal conductivity of soils. Ph.D. diss. Norwegian Univ. of Science and Technol., Trondheim (CRREL draft transl. 637, 1977).

Kasubuchi, T., Momose, T., Tsuchiya, F., Tarnawski, V.R., 2007. Normalized thermal conductivity model for three Japanese soils. Trans. Jpn. Soc. Irrig. Drain. Rural. Eng. 75, 529–533.

Kersten, M.S. 1949. Laboratory research for the determination of the thermal properties of soils. ACFEL Tech. Rep. 23. Univ. of Minnesota, Minneapolis.

Kojima, Y., Kawashima, T., Noborio, K., Kamiya, K., Horton, R., 2021. A dual-probe heat pulse-based sensor that simultaneously determines soil thermal properties, soil water content and soil water matric potential. Comput. Electron. Agr 188, 106331. https://doi.org/10.1016/j.compag.2021.106331.

Li, K.-Q., Kang, Q., Nie, J.-Y., Huang, X.-W., 2022. Artificial neural network for predicting the thermal conductivity of soils based on a systematic database. Geothermics 103, 102416. https://doi.org/10.1016/j.geothermics.2022.102416.

Lu, N., Dong, Y., 2015. Closed-form equation for thermal conductivity of unsaturated soils at room temperature. J. Geotech. Geoenviron. 141, 04015016. https://doi.org/10.1061/(asce)gt.1943-5606.0001295.

Lu, S., Ren, T., Gong, Y., Horton, R., 2007. An Improved Model for Predicting Soil Thermal Conductivity from Water Content at Room Temperature. Soil. Sci. Soc. Am. J 71, 8–14. https://doi.org/10.2136/sssaj2006.0041.

McInnes, K.J., 1981. Thermal conductivities of soils from dryland wheat regions of Eastern Washington (Master dissertation). Washington State University, Pullman, WA.

Minasny, B., McBratney, A.B., 2018. Limited effect of organic matter on soil available water capacity. Eur. J. Soil. Sci. 69, 39–47. https://doi.org/10.1111/ejss.12475.

Mochizuki, H., Sakaguchi, I., Inoue, M., 2003. Comparison of the methods measuring of soil thermal conductivity. J. Jpn. Soc. Soil. Phys. 93, 47–50.

McCombie, M.L., Tarnawski, V.R., Bovesecchi, G., Coppa, P., Leong, W.H., 2016. Thermal Conductivity of Pyroclastic Soil (Pozzolana) from the Environs of Rome. Int. J. Thermophys 38, 21. https://doi.org/10.1007/s10765-016-2161-y.

Ng, W., Minasny, B., Mendes, W. de S., Demattê, J.A.M., 2020. The influence of training sample size on the accuracy of deep learning models for the prediction of soil

properties with near-infrared spectroscopy data. SOIL 6, 565–578. https://doi.org/10.5194/soil-6-565-2020.
Nikolaev, I.V., Leong, W.H., Rosen, M.A., 2013. Experimental investigation of soil thermal conductivity over a wide temperature range. Int. J. Thermophys 34, 1110–1129. https://doi.org/10.1007/s10765-013-1456-5.
Navidi, M.N., Seyedmohammadi, J., Jalali, S.A.S., 2022. Predicting soil water content using support vector machines improved by meta-heuristic algorithms and remotely sensed data. Géoméch. Geoengin. 17, 712–726. https://doi.org/10.1080/17486025.2020.1864032.
Paszke, A., Gross, S., Massa, F., Lerer, A., Bradbury, J., Chanan, G., Killeen, T., Lin, Z., Gimelshein, N., Antiga, L., 2019. Pytorch: An imperative style, high-performance deep learning library. In: Advances in neural information processing systems, pp. 8026–8037. https://arxiv.org/abs/1912.01703.
Poggio, L., de Sousa, L.M., Batjes, N.H., Heuvelink, G.B.M., Kempen, B., Ribeiro, E., Rossiter, D., 2021. SoilGrids 2.0: producing soil information for the globe with quantified spatial uncertainty. SOIL 7, 217–240. https://doi.org/10.5194/soil-7-217-2021.
Prechelt, L., 1998. Early stopping - but when? In: Orr, G.B., Müller, K.R. (Eds.), Neural Networks: Tricks of the Trade. Lecture Notes in Computer Science. 1524. Springer, Berlin, Heidelberg.
Rudiyanto, Minasny, B., Chaney, N.W., Maggi, F., Giap, S.G.E., Shah, R.M., Fiantis, D., Setiawan, B.I., 2021. Pedotransfer functions for estimating soil hydraulic properties from saturation to dryness. Geoderma 403, 115194. doi: 10.1016/j.geoderma.2021.115194.
Saadat, S., Seyedmohammadi, J., Esmaeelnejad, L., 2018. Selection of a suitable soft computing model for estimation of soil cation exchange capacity. Commun. Soil. Sci. Plant. Anal. 49, 2664–2679. https://doi.org/10.1080/00103624.2018.1526952.
Sadeghi, M., Ghanbarian, B., Horton, R., 2018. Derivation of an explicit form of the percolation-based effective-medium approximation for thermal conductivity of partially saturated soils. Water. Resour. Res 54, 1389–1399. https://doi.org/10.1002/2017wr021714.
Schjønning, P., 2021. Thermal conductivity of undisturbed soil – Measurements and predictions. Geoderma 402, 115188. https://doi.org/10.1016/j.geoderma.2021.115188.
Shen, C., Appling, A.P., Gentine, P., Bandai, T., Gupta, H., Tartakovsky, A., Baity-Jesi, M., Fenicia, F., Kifer, D., Li, L., Liu, X., Ren, W., Zheng, Y., Harman, C.J., Clark, M., Farthing, M., Feng, D., Kumar, P., Aboelyazeed, D., Rahmani, F., Song, Y., Beck, H.E., Bindas, T., Dwivedi, D., Fang, K., Höge, M., Rackauckas, C., Mohanty, B., Roy, T., Xu, C., Lawson, K., 2023. Differentiable modelling to unify machine learning and physical models for geosciences. Nat. Rev. Earth. Environ. 1–16. https://doi.org/10.1038/s43017-023-00450-9.
Sodini, M., Cacini, S., Navarro, A., Traversari, S., Massa, D., 2024. Estimation of pore-water electrical conductivity in soilless tomatoes cultivation using an interpretable machine learning model. Comput. Electron. Agric. 218. https://doi.org/10.1016/j.compag.2024.108746.
Tarnawski, V.R., McCombie, M.L., Momose, T., Sakaguchi, I., Leong, W.H., 2013. Thermal conductivity of standard sands. part iii. full range of saturation. Int. J. Thermophys. 34, 1130–1147. https://doi.org/10.1007/s10765-013-1455-6.
Tarnawski, V.R., Momose, T., McCombie, M.L., Leong, W.H., 2015. Canadian field soils III. Thermal-conductivity data and modeling. Int. J. Thermophys 36, 119–156. https://doi.org/10.1007/s10765-014-1793-z.
Tarnawski, V.R., Tsuchiya, F., Coppa, P., Bovesecchi, G., 2019. Volcanic soils: Inverse modeling of thermal conductivity data. Int. J. Thermophys 40, 14. https://doi.org/10.1007/s10765-018-2480-2.
Tokoro, T., Ishikawa, T., Shirai, S., Nakamura, T., 2016. Estimation methods for thermal conductivity of sandy soil with electrical characteristics. Soils. Found 56, 927–936. https://doi.org/10.1016/j.sandf.2016.08.016.
Tuller, M., Or, D., Dudley, L.M., 1999. Adsorption and capillary condensation in porous media: Liquid retention and interfacial configurations in angular pores. Water. Resour. Res 35, 1949–1964. https://doi.org/10.1029/1999wr900098.
van Genuchten, M.T., 1980. A closed-form equation for predicting the hydraulic conductivity of unsaturated soils. Soil. Sci. Soc. Am. J 44, 892–898. https://doi.org/10.2136/sssaj1980.03615995004400050002x.
Van Looy, K., Bouma, J., Herbst, M., Koestel, J., Minasny, B., Mishra, U., Montzka, C., Nemes, A., Pachepsky, Y.A., Padarian, J., Schaap, M.G., Tóth, B., Verhoef, A., Vanderborght, J., Ploeg, M.J., Weihermüller, L., Zacharias, S., Zhang, Y., Vereecken, H., 2017. Pedotransfer functions in earth system science: Challenges and perspectives. Rev. Geophys 55, 1199–1256. https://doi.org/10.1002/2017rg000581.
Vereecken, H., Amelung, W., Bauke, S.L., Bogena, H., Brüggemann, N., Montzka, C., Vanderborght, J., Bechtold, M., Blöschl, G., Carminati, A., Javaux, M., Konings, A.G., Kusche, J., Neuweiler, I., Or, D., Steele-Dunne, S., Verhoef, A., Young, M., Zhang, Y., 2022. Soil hydrology in the Earth system. Nat. Rev. Earth. Environ 1–15. https://doi.org/10.1038/s43017-022-00324-6.
Xiao, C., Ji, Q., Chen, J., Zhang, F., Li, Y., Fan, J., Hou, X., Yan, F., Wang, H., 2023. Prediction of soil salinity parameters using machine learning models in an arid region of northwest China. Comput. Electron. Agr 204, 107512. https://doi.org/10.1016/j.compag.2022.107512.
Zhang, N., Zou, H., Zhang, L., Puppala, A.J., Liu, S., Cai, G., 2020a. A unified soil thermal conductivity model based on artificial neural network. Int. J. Therm. Sci. 155, 106414. https://doi.org/10.1016/j.ijthermalsci.2020.106414.
Zhang, T., Wang, C., Liu, S., Zhang, N., Zhang, T.-W., 2020b. Assessment of soil thermal conduction using artificial neural network models. Cold. Reg. Sci. Technol. 169, 102907. https://doi.org/10.1016/j.coldregions.2019.102907.
Zhang, Y., Schaap, M.G., 2017. Weighted recalibration of the Rosetta pedotransfer model with improved estimates of hydraulic parameter distributions and summary statistics (Rosetta3). J. Hydrol 547, 39–53. https://doi.org/10.1016/j.jhydrol.2017.01.004.
Zhao, H., Zeng, Y., Lv, S., Su, Z., 2018. Analysis of soil hydraulic and thermal properties for land surface modeling over the Tibetan Plateau. Earth. Syst. Sci. Data 10, 1031–1061. https://doi.org/10.5194/essd-10-1031-2018.
Zhao, Y., Si, B., Zhang, Z., Li, M., He, H., Hill, R.L., 2019. A new thermal conductivity model for sandy and peat soils. Agr. Forest. Meteorol 274, 95–105. https://doi.org/10.1016/j.agrformet.2019.04.004.